Pharmacological Reports (2022) 74:241–247
https://doi.org/10.1007/s43440-021-00311-6

SHORT COMMUNICATION

In vivo evaluation of a microtubule PET ligand, [^{11}C]MPC-6827, in mice following chronic alcohol consumption

J. S. Dileep Kumar[1,2] · Andrei Molotkov[3] · Michael C. Salling[4] · Patrick Carberry[3] · Jaya Prabhakaran[1,5] · John Castrillon[3] · Akiva Mintz[1,3]

Received: 8 April 2021 / Revised: 8 July 2021 / Accepted: 13 July 2021 / Published online: 7 September 2021

Abstract

Background Excessive alcohol consumption is a global health burden and requires a better understanding of its neurobiology. A lower density of brain microtubules is found in alcohol-related human brain disease postmortem and in rodent models of chronic alcohol consumption. Here, we report in vivo imaging studies of microtubules in brain using our recently reported Positron Emission Tomography (PET) tracer, [^{11}C]MPC-6827, in chronic alcohol-consuming adult male C57BL/6 J mice and control mice.

Methods In vivo PET imaging studies of [^{11}C]MPC-6827 (3.7 ± 0.8 MBq) were performed in two groups of adult male mice: (1) water-consuming control mice ($n = 4$) and (2) mice that consumed 20% alcohol (w/v) for 4 months using the intermittent 2-bottle choice procedure that has been shown to lead to signs of alcohol dependence. Dynamic 63 min PET images were acquired using a microPET Inveon system (Siemens, Germany). PET images were reconstructed using the 3D-OSEM algorithm and analyzed using VivoQuant version 4 (Invicro, MA). Tracer uptake in ROIs that included whole brain, prefrontal cortex (PFC), liver and heart was measured and plotted as %ID/g over time (0–63 min) to generate time-activity curves (TACs).

Results In general, a trend for lower binding of [^{11}C]MPC-6827 in the whole brain and PFC of mice in the chronic alcohol group was found compared with control group. No group difference in radiotracer binding was found in the peripheral organs such as liver and heart.

Conclusions This pilot study indicates a trend of loss of microtubule binding in whole brain and prefrontal cortex of chronic alcohol administered mice brain compared to control mice, but no loss in heart or liver. These results indicate the potential of [^{11}C]MPC-6827 as a PET ligand for further in vivo imaging investigations of AUD in human.

Keywords PET · Microtubule · Alcoholism · Tubulin · Brain

Abbreviations

Aβ	Amyloid beta
AD	Alzheimer's disease
ALS	Amyotrophic lateral sclerosis
AUD	Alcohol use disorder
BBB	Blood brain barrier
IA	Intermittent access
ID/g	Injected dose/gram
MBq	Mega becquerel
MT	Microtubule
PET	Positron emission tomography
PFC	Prefrontal cortex
PTM	Post-translational modifications
TAC	Time-activity curves
SEM	Standard error of the mean
SUV	Standardized uptake values
W/v	Weight per volume

✉ J. S. Dileep Kumar
dkumar7@northwell.edu

1 Area of Molecular Imaging and Neuropathology, New York State Psychiatric Institute, Manhattan, NY, USA

2 Feinstein Institutes for Medical Research, North Shore University Hospital, Manhasset, New York, USA

3 Department of Radiology, Columbia University Medical Center, Manhattan, NY, USA

4 Department of Cell Biology and Anatomy, Louisiana State University Health Sciences Center, New Orleans, LA, USA

5 Department of Psychiatry, Columbia University Medical Center, New York, NY, USA

Introduction

Over 14 million adults aged 18 and older, representing 5.8% of this population in the US suffer from Alcohol Use Disorder (AUD) [1]. Nearly half a million adolescents aged 12–17 years have AUD [1]. An estimated that 88,000 people die from alcohol-related causes annually, making alcohol the third leading preventable cause of death in the United States and fifth leading risk factor for premature death and disability globally [1]. Major effects of alcohol in the body are observed in brain, liver, heart, pancreas, and immune responses [2]. Chronic alcohol consumption is a risk factor for cancer and dementia [2–4]. There is an unmet need for identifying new drug targets for this disease [5–7]. The lack of a validated biomarker for mapping clinical state of AUD also hamper drug development.

Loss of tubulins, the major repeating protofilament units of α- and β-tubulin heterodimers of the microtubule (MT) cytoskeleton has been reported in brain in response to chronic excessive alcohol exposure and is a potential biomarker for AUD [8–11]. Loss of α- and β-tubulins and spectrin β-II proteins are reported in human postmortem brain in AUD [8]. However, no changes were found in actin proteins in alcoholic subjects compared with controls [8]. Among the tested regions in alcohol group, prefrontal cortex (PFC) shows highest α- and β-tubulin loss (50 and 47%), followed by hippocampus (54%, 36%), cerebellum (54%, 34%), and caudate nucleus (30%, 31%) in comparison to control group [6]. However, this effect was not observed with non-alcoholic suicide patients. Similar to the findings in postmortem human brain, 47% reduction of α-tubulins and 38% reduction of β-tubulin brain protein levels are reported in chronic alcohol administered rodents [8–11]. Although alcohol-related pathology in brain differs from that of peripheral organs, tubulin alterations are also reported in liver and heart of AUD patients [12, 13].

Postmortem tubulin disruption may compromise findings in brain and periphery organs in AUD. Positron Emission Tomography (PET) imaging of MT with radiolabeled and blood brain barrier (BBB) penetrating MT ligands may offer a direct approach for detecting and quantifying the changes in MT density, in vivo, in brain and other organs. [^{11}C]MPC-6827 is a high affinity, selective MT ligand that binds to tubulins at the colchicine site [14, 15]. It is the first PET ligand that showed BBB penetration and specific binding in brain and periphery organs in rodents [14, 15]. Our pilot preclinical PET imaging studies of [^{11}C]MPC-6827 in and Alzheimer's Disease (AD) mice model of Aβ pathology (5×FAD), tau pathology (rTg4510), and Amyotrophic Lateral Sclerosis (ALS) pathology (SOD1*G93A) detected lower binding in brain compared to wild type mice [16]. This finding indicates that disease-related tubulin loss may be measurable by PET imaging. We now report use of [^{11}C]MPC-6827 to determine MT alterations in mice following long-term consumption of alcohol compared to age-matched water-consuming control mice using microPET imaging (Fig. 1).

Materials and methods

All commercial chemicals and solvents used in the synthesis were purchased from Sigma–Aldrich Chemical Co., (St. Louis, MO), or Fisher Scientific Inc., (Springfield, NJ) and were used without further purification. Gamma-ray detector (Bioscan Flow-Count fitted with a NaI detector) coupled in series with the UV detector (Waters Model 996 set at λ 254 nm) was used for detection of radiolabeled products. Data acquisition for both the analytical and preparative systems was accomplished using a Waters Empower Chromatography System. MPC-6827 and desmethyl-MPC-6827 were synthesized according as previously reported [14]. [^{11}C]CO_2 was produced from a Siemens Eclipse cyclotron. Radiosynthesis of [^{11}C]MPC-6827 was achieved by reacting corresponding desmethyl-MPC-6827 phenolate with [^{11}C]CH_3I in a GE-FX2MeI/FX2M radiochemistry module using our established procedure [14–16]. All animal experimental procedures were carried out in accordance with the Institutional Animal Care Committee ethical guidelines of Columbia University Medical Center. All experiments were performed in male C57BL⁄6 J mice (Jackson Laboratories, Bar Harbour, ME) during adolescence and adulthood (postnatal day 35–120).

Chronic alcohol treated mice

The chronic intermittent alcohol consumption model used was based on a previously reported and widely used procedure [17]. This method of alcohol exposure was chosen as it is a voluntary, approximates binge drinking levels and states of withdrawal, can lead to signs of alcohol dependence, and is known to model alcohol induced neuroadaptations observed in humans like increased glutamatergic neurotransmission [17]. In short, mice were given either two bottles of water ($n = 4$) or intermittent access to alcohol

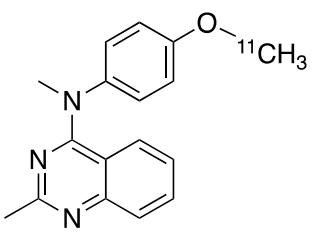

Fig. 1 Chemical structure of [^{11}C]MPC-6827

(IA) ($n = 4$) which consisted of one bottle of water and one bottle of increasing concentrations of alcohol (5, 10, 15% w/v) over the first three sessions and then maintained on 20% (w/v) alcohol throughout the rest of the experiment. A cage with bottles and no mice was placed on the rack to estimate loss of fluid. Mice and bottles were weighed daily to calculate alcohol dose consumed (g/kg) and alcohol preference (%) after subtracting bottle drip. This procedure is known to result in elevated blood alcohol levels and signs of withdrawal in C57BL/6 J mice [17]. Both mice groups ($n = 4$) underwent PET scans and imaging occurred one day after last session of alcohol consumption.

microPET imaging

microPET imaging studies were performed in anesthetized (by isoflurane 5% induction; O_2 rate: 2 L/min) mice using our established procedure [14–16]. PET imaging studies were conducted on a Siemens Inviorn microPET by tail vein administration of [^{11}C]MPC-6827 (1.85 ± 0.37 MBq, 20 µL volume) and dynamic acquisition was for 63 min in multiple frames (2 × 30 s, 4 × 60 s, 3 × 120 s, 4 × 180 s, and 4 × 300 s). Using VivoQuant (ver 4, Invicro, MA) software (version 4.0, Switzerland), three-dimensional ellipsoid volume of interests (VOIs) ranging from 2 to 6 mm^3 were placed manually at the center of the brain, heart (blood-pool), and liver. The percentage of injected dose/gram (%ID/g) was estimated using a calibration factor calculated from a phantom study, and time-activity curves (TACs) and standardized uptake values (SUV) were derived from VOIs.

Statistical analyses

All data reported are as mean ± standard error of the mean (SEM), unless otherwise stated. Statistical analyses of radiotracer binding in the whole brain, PFC, heart and liver regions in control and chronic alcohol treated mice groups were analyzed using an Mann–Whitney nonparametric test. Statistical analyses were performed using Graphpad Prism version 9.1.0. Graphs were made using Graphpad Prism version 9.1.0. A p value less than 0.05 was considered statistically significant.

Results

Radiosynthesis of [^{11}C]MPC-6827 was accomplished with 45 ± 5% radiochemical yield and molar activity of 100 ± 37 GBq/µmol at end of synthesis. After 2 weeks, mice given IA to ethanol achieved > 15 g/kg/24 h on average, which is likely to lead to blood alcohol concentrations above 80 mg/dl [18] (Fig. 2). We also found a similar trend for ethanol consumption throughout the remaining sessions (~ 12–20 g/kg/24 h) (Fig. 2).

The dynamic microPET images of [^{11}C]MPC-6827 showed BBB penetration and retention of radiotracer in brain of both chronic alcohol administered mice and water-consuming control mice (Fig. 3).

As evident from Fig. 3, alcohol-consuming mice showed a lower binding in whole brain (right image) compared to control (left image). Similarly, whole brain TACs also demonstrate reduced binding of [^{11}C]MPC-6827 in alcohol mice group compared to control mice (Fig. 4A). The radioligand exhibited somewhat heterogeneous distribution in brain with a higher retention in cortical regions. TACs in PFC indicate reduced binding of the tracer (Fig. 4B) in the alcohol group compared to control. The peak uptake of tracer is comparable for whole brain and PFC in both groups. SUV analyses show lower binding of tracer (~ 20%) in whole brain and PFC in alcohol group than control

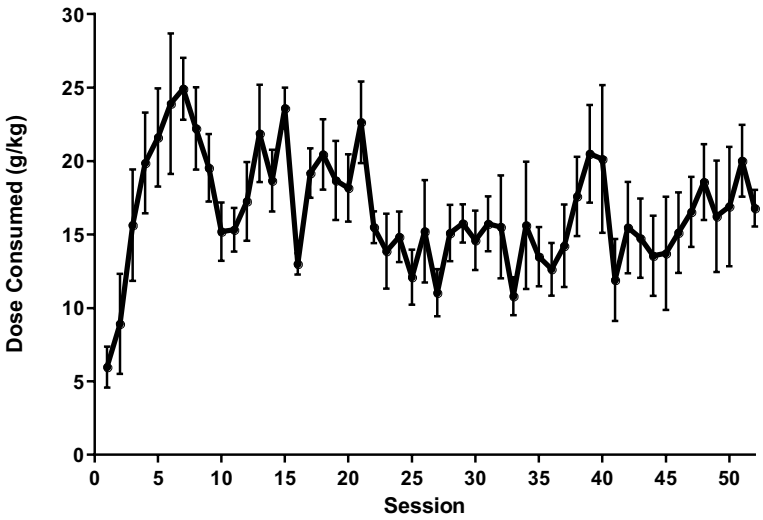

Fig. 2 Ethanol consumption (g/kg) over 24 h for C57BL/6 J mice given intermittent access to alcohol. Values are reported as the mean ± standard error of the mean (SEM) from four of mice per time point

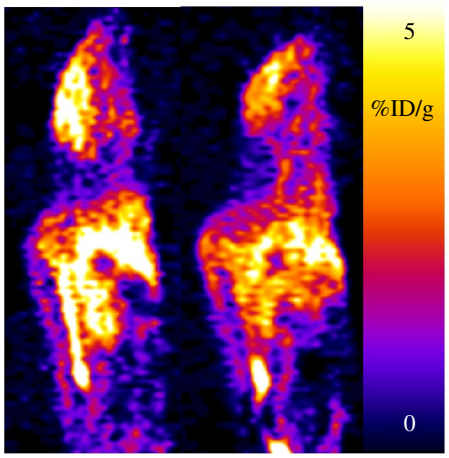

Fig. 3 Representative microPET (sagittal) image, computed from 0 to 63 min, summed images of [^{11}C]MPC-6827 in control male white mice ($n = 4$, left) and alcohol-consuming mice group ($n = 4$, right). Image represents our observation that the alcohol treated group exhibited less binding of tracer compared to controls

group (Fig. 5A, B). Statistical analyses of whole brain SUV data show no significantly different binding of radiotracer between water (median = 0.88, $n = 4$) and chronic alcohol (median = 0.75, $n = 4$) conditions (Mann–Whitney test, $U = 3$, $p = 0.2$), whereas, a noticeable trend for significance of PFC SUV data between water (median = 1.07, $n = 4$) and chronic alcohol (median = 0.89, $n = 4$) groups (Mann–Whitney, $U = 1$, $p = 0.0571$).

Subsequently, we examined the binding of [^{11}C]MPC-6827 in heart and liver of chronic alcohol treated and water treated mice. The uptake of [^{11}C]MPC-6827 in heart was peaked at 1 min followed by a fast washout for both groups (Fig. 6A). Whereas, liver uptake was peaked at 3 min, followed by a fast washout up to 18 min, then a slow decline in activity throughout the remaining scan period (Fig. 6B). The uptake and SUV of [^{11}C]MPC-6827 in heart and liver did not show any statistically significant group binding differences (Mann–Whitney test, heart: $U = 8$, $p > 0.99$; liver: $U = 8$, $p > 0.99$).

Discussion

The present study reports the first preclinical in vivo imaging of chronic alcohol-consuming mice and control water-consuming mice with PET using an MT targeting radioligand. We adopted an established intermittent access method to induce high chronic ethanol intake in mice because this model mimics the features of human alcohol dependence [17, 18]. Similar to rodents, the intermittent access procedure also results in an escalation of voluntary alcohol drinking in non-human primates [19]. This procedure is relatively simple, highly valid, and offers translational value among other models and appears to be a useful procedure for preclinical evaluation of potential therapeutic approaches against AUD. Several PET tracers of different imaging targets are being evaluated for PET imaging of human AUD [20–22]. Although these tracers show proof of concept of imaging AUD in human, most of them show moderate to minumum effect size, as well as mixed or conflicting results. The above tracers also are not proven successful in correlating with clinical finding to predict treatment responses, and no/less data available differentiate the various stages of AUD. Since loss of cortical thickness due to reduced MT stability is a pathogenic finding in AUD, visualizing this effect in vivo via PET imaging in various stages of AUD could have significant value in terms of studying pathophysiology and identifying treatment targets. If MT density quantified by PET imaging were correlated with symptomatology in future human research, further studies could examine this biomarker in relationship to treatment outcome in treatment studies, and potentially as a biomarker for drug development. A large number of epigenetic, post-translational

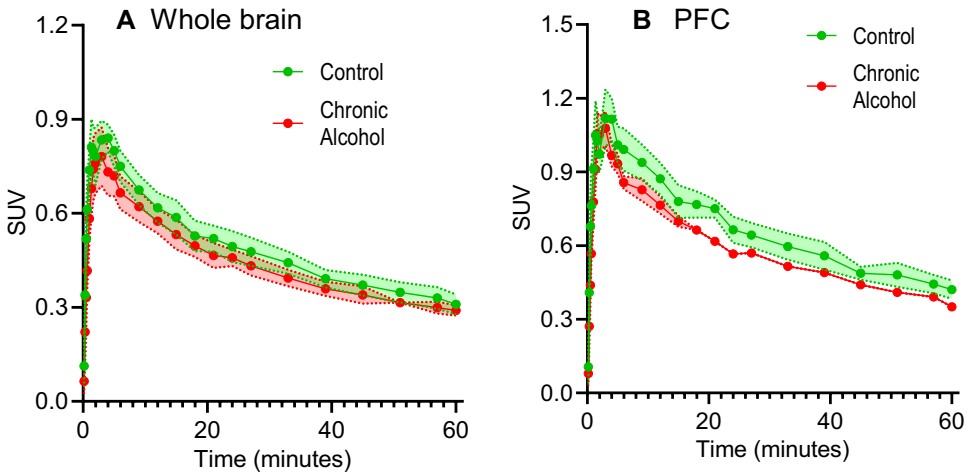

Fig. 4 Time-activity curves of [^{11}C]MPC-6827 binding in control water-consuming and chronic alcohol-consuming mice. **A** Whole brain; **B** prefrontal cortex. Values are reported as the mean (solid line) ± SEM (dotted line) from four pairs of mice per group. Radioactivity in whole brain and prefrontal cortex of alcohol treated mice group suggest less binding of tracer compared to controls

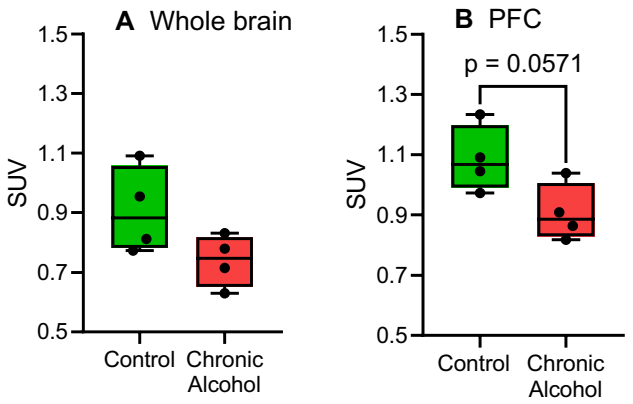

Fig. 5 Standardized uptake values of [11C]MPC-6827 binding in control and chronic alcohol-consuming mice. **A** Whole brain; **B** prefrontal cortex. Values are reported as a box and whisker plot where from four pairs of mice per group. Whole brain SUV values were not significantly different between water (median = 0.88, $n = 4$) and chronic alcohol (median = 0.75, $n = 4$) conditions (Mann–Whitney test, $U = 3$, $p = 0.2$). However, PFC, there was a nearly significant reduction in SUV (Mann–Whitney, $U = 1$, $p = 0.057$) between water (median = 1.07, $n = 4$) and chronic alcohol (median = 0.89, $n = 4$) groups

modifications (PTM) and environmental factors contribute to MT or tubulin loss in AUD [9, 23, 24]. Therefore, cumulative loss of MT is a common pathway for a variety of biochemical pathologies leading to AUD. Furthermore, MTs and tubulins are highly expressed in brain compared to other currently available PET imaging targets for AUD. This offers a likelihood of higher brain uptake and significant binding difference of MT targeted PET tracer in AUD compared to control group. Hence monitoring the changes in MT, in vivo, in brain may also be advantageous for understanding its involvement in the pathophysiology of AUD. Imaging experiments were performed with [11C]MPC-6827, a PET tracer that exhibited specific binding to MT in brain, developed by our group [14–16]. MPC-6827 is a known MT depolymerization inhibitor which binds mostly to the colchicine sites of α, and β-tubulin at MT exchangeable site and to sites of α-tubulin residues at non-exchangeable sites [25, 26]. A large number of epigenetic, post-translational modifications (PTM) and environmental factors contribute to MT or tubulin loss in AUD [9, 25, 26].

The PET scans (Figs. 3, 4, 5) show a trend of lower binding of [11C]MPC-6827 in whole brain and PFC of chronic ethanol administered mice compared with water-administered control mice. This finding is in agreement with lower binding to tubulins determined by in vitro postmortem studies and also the findings in animal models of AUD [8–11]. However, in vitro studies show tubulin loss in heart and liver in contrast to our findings with in vivo PET imaging. This may be partially due to a methodological difference, because MT lose structure in vitro and so PET may offer a different in vivo result to postmortem brain tissue. In vitro methods measure binding of tubulins based on specific antibodies, whereas, PET detects the sum of the available α- and β-tubulin variants and PTM of MT which may be up or down regulated in AUD. For example, acetylated-tubulins are upregulated in AUD compared to α- and β-tubulins [8]. Currently, we do know whether binding of [11C]MPC-6827 is to all tubulin variants and or MT-PTMs. It is also difficult to determine the in vivo selectivity of [11C]MPC-6827 for tubulins and MT-PTMs due to the lack of specific brain penetrating ligands to use as nonspecific binding agents. Furthermore, the sensitivity of in vitro methods may be higher compared with in vivo PET.

Apart from PFC binding, we did not perform regional binding analysis of the tracer in other brain regions due to low spatial resolution of microPET coupled with the high retention of [11C]MPC-6827. This microPET imaging study on mice also lacks arterial input function measurements and partial volume correction derived measurement of tracer binding in brain. Such methods are not practical for mice studies due to smaller brain size and volume of blood.

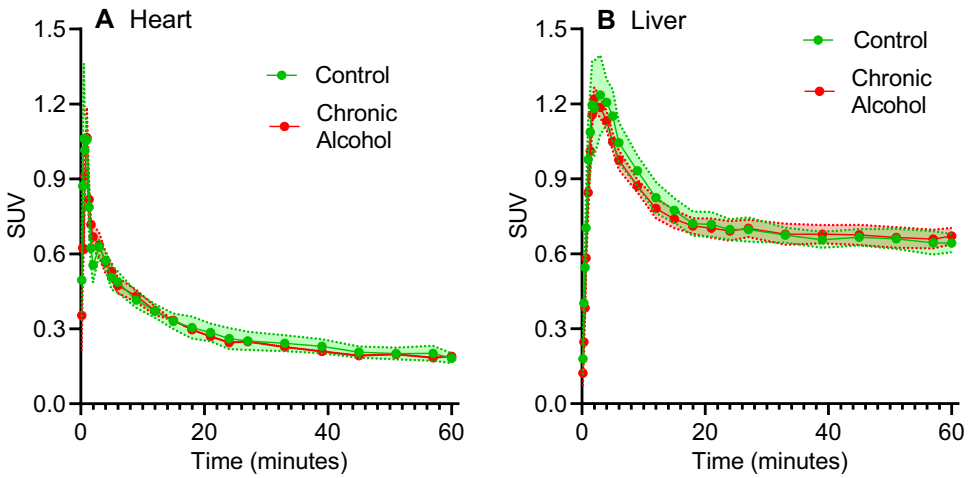

Fig. 6 Time-activity curves of [11C]MPC-6827 in control mice and chronic alcohol consuming mice in heart (**A**) and liver (**B**). Values are reported as the mean ± SEM from four pairs of mice per group. Radiotracer did not show any significant differences of binding in the heart and liver

Since both mice group and conditions exhibited comparable peak uptake of radiotracer in whole brain and PFC, the %ID/g as outcome measurement for tracer binding comparison is acceptable. In addition to brain, heart also exhibited comparable peak uptake of the tracer in both groups further support the validity of %ID/g as the tracer binding outcome.

Although tubulin pathology is present in liver and heart of AUD patients, we did not find significant difference in [^{11}C]MPC-6827 binding in the hearts of alcohol treated mice and control group. This is likely due to the duration of alcohol exposure (months in a mouse versus decades in a human) and potentially be accelerated using intermittent alcohol vapor exposure known to accelerate signs of dependence in mice. It also may be due to different variants of tubulins and or PTM of tubulins in periphery organs compared to brain. We found modest specific binding of [^{11}C]MPC-6827 in liver in both groups of mice. There was very less specific binding of the radioligand in heart, and, therefore, most of the cardiac binding may also be partially due to a blood flow effect of radiotracer [14]. The higher retention of radiotracer in liver may also be due to an accumulation of radioactive metabolites of [^{11}C]MPC-6827 [14].

Conclusions

In conclusion, our pilot preclinical imaging studies show a trend of reduction of whole brain and PFC uptake with MT targeted PET tracer [^{11}C]MPC-6827 in chronic alcohol-consuming mice group compared to water-consuming control mice. This result supports the previous report of lower binding of α- and β-tubulins in AUD in human brain (postmortem) and also in vitro findings in animal models of alcoholism. The major limitations of these studies are the variations of alcohol uptake in mice, the lack of plasma input data and large sample size. Therefore, further PET imaging studies with AUD in non-human primates or human subjects and control with arterial input functions are required to establish the potential of [^{11}C]MPC-6827 as a potential PET tracer for mapping brain MT in AUD and related diseases.

Author contributions JSDK conceived the idea. JSDK, MCS, and AM designed the experiments. JSDK, MCS, AM, PC, JP, and JC performed the experiments. JSDK, AM, and MCS performed all analyses. JSDK, AM, MCS, and AM analyzed and interpret the data. JSDK drafted the manuscript. The manuscript was written through contributions of all authors and all authors have given approval to the final version of the manuscript.

Funding This work was Funded by NCATS UL1TR001873 (Reilly) Irving Institute/CTSA Translational Therapeutics Accelerator.

Declarations

Conflicts of interest The authors declare no conflicts of interest.

References

1. https://www.samhsa.gov/data/sites/default/files/cbhsqreports/NSDUHNationalFindingsReport2018/NSDUHNationalFindingsReport2018.pdf.
2. Barve S, Chen S-Y, Kirpich I, Watson WH, McClain C. Development prevention, and treatment of alcohol-induced organ injury: the role of nutrition. Alcohol Res. 2017;38(2):289–302.
3. Scheideler JK, Klein WMP. Awareness of the link between alcohol consumption and cancer across the world: a review. Cancer Epidemiol Biomarkers Prev. 2018;27(4):429–37.
4. Sabia S, Fayosse A, Dumurgier J, Dugravot A, Akbaraly T, Britton A, Kivimaki M, Singh MA. Alcohol consumption and risk of dementia: 23 year follow-up of Whitehall II cohort study. BMJ. 2018;362:k2927.
5. Ray LA, Bujarski S, Grodin E, Hartwell E, Green R, Venegas A, Lim AC, Gillis A, Miotto K. State-of-the-art behavioral and pharmacological treatments for Alcohol Use Disorder. Am J Drug Alcohol Abuse. 2019;45(2):124–40.
6. Cannella N, Ubaldi M, Masi A, Bramucci M, Roberto M, Bifone A, Ciccocioppo R. Building better strategies to develop new medications in Alcohol Use Disorder: learning from past success and failure to shape a brighter future. Neurosci Biobehav Rev. 2019;103:384–98.
7. Williams EC, Matson TE, Harris AHS. Strategies to increase implementation of pharmacotherapy for alcohol use disorders: a structured review of care delivery and implementation interventions. Addict Sci Clin Pract. 2019;14:6.
8. Erdozain AM, Morentin B, Bedford L, King E, Tooth D, Brewer C, et al. Alcohol-related brain damage in humans. PLoS ONE. 2014;9(4):e93586.
9. Labisso WL, Raulin A-C, Nwidu LL, Kocon A, Wayne D, Erdozain AM, et al. The loss of alpha- and beta-tubulin proteins are a pathological hallmark of chronic alcohol consumption and natural brain ageing. Brain Sci. 2018;8(9):175.
10. Smith KJ, Butler TR, Prendergast MA. Ethanol impairs microtubule formation via interactions at a microtubule associated protein-sensitive site. Alcohol. 2013;47(7):539–43.
11. Enculescu C, Kerr ED, Benjamin YKY, Schenk G, Fortes MRS, Schulz BL. Proteomics reveals profound metabolic changes in the alcohol use disorder brain. ACS Chem Neurosci. 2019;10(5):2364.
12. Shepard BD, Tuma PL. Alcohol-induced alterations of the hepatocyte cytoskeleton. World J Gastroenterol. 2010;16(11):1358–65.
13. Piano MR, Phillips SA. Alcoholic cardiomyopathy: pathophysiologic insights. Cardiovasc Toxicol. 2014;14(4):291–308.
14. Kumar JSD, Solingapuram SKK, Prabhakaran J, Oufkir HR, Ramanathan G, Whitlow CT, et al. Radiosynthesis and In vivo evaluation of [^{11}C]MPC-6827, the first brain penetrant microtubule PET ligand. J Med Chem. 2018;61(5):2118–23.
15. Kumar JSD, Prabhakaran J, Damuka N, Hines JW, Norman S, Meghana DM, et al. In vivo comparison of N-11CH3 vs O-11CH3 radiolabeled microtubule targeted PET ligands. Bioorg Med Chem Let. 2010;30(2):126785.
16. Kumar JSD, Prabhakaran J, Kim J, Castrillon J, Molotkov A, Dileep H, et al. In vivo evaluation of microtubule PET ligand [^{11}C]MPC-6827 in animal models of neurodegenerative disorders. J Nucl Med. 2019;60:1301 (s1).
17. Hwa LS, Chu A, Levinson SA, Kayyali TM, DeBold JF, Miczek KA. Persistent escalation of alcohol drinking in C57Bl/6J mice

with intermittent access to 20% ethanol. Alcohol Clin Exp Res. 2011;35(11):1938.
18. Salling MC, Skelly MJ, Avegno E, Regan S, Zeric T, Nichols E, Harrison NL. Alcohol consumption during adolescence in a mouse model of binge drinking alters the intrinsic excitability and function of the prefrontal cortex through a reduction in the hyperpolarization-activated cation current. J Neurosci. 2018;38(27):6207–22.
19. Lindell SG, Schwandt ML, Suomi SJ, Rice KC, Heilig M, Barr CS. Intermittent access to ethanol induces escalated alcohol consumption in primates. J Addict Behav Ther Rehabil. 2017;6(1):163.
20. Laere KV, Ceccarini J. How acute and chronic alcohol consumption modulate multiple neurotransmitter systems: a review of clinical PET neuroimaging. J Alcohol Drug Depend. 2018;6:2.
21. Wiers CE, Cabrera E, Skarda E, Volkow ND, Wang G-J. PET imaging for addiction medicine: from neural mechanisms to clinical considerations. Prog Brain Res. 2016;224:175.
22. Solingapuram Sai KK, Hurley RA, Dodda M, Taber KH. Positron emission tomography: updates on imaging of addiction. J Neuropsychiatry Clin Neurosci. 2019;31:4.
23. Smith SL, Jennett RB, Sorrell MF, Tuma DJ. Acetaldehyde substoichiometrically inhibits bovine neurotubulin polymerization. J Clin Investig. 1989;84:337.
24. Skultetyova L, Ustinova K, Kutil Z, Novakova Z, Pavlicek J, Mikesova J, et al. Human histone deacetylase 6 shows strong preference for tubulin dimers over assembled microtubules. Sci Rep. 2017;7:11547.
25. Kasibhatla S, Baichwal V, Cai SX, Roth B, Skvortsova I, Skvortsov S, et al. MPC-6827: a small-molecule inhibitor of microtubule formation that is not a substrate for multidrug resistance pumps. Cancer Res. 2007;67(12):5865–71.
26. Yan W, Yang T, Yang J, Wang T, Yu Y, Wang Y, et al. SKLB060 reversibly binds to colchicine site of tubulin and possesses efficacy in multidrug-resistant cell lines. Cell Physiol Biochem. 2018;47:489–504.